Hindawi
International Journal of Aerospace Engineering
Volume 2018, Article ID 9237907, 16 pages
https://doi.org/10.1155/2018/9237907

Research Article

Performance Analysis of a Three-Stream Adaptive Cycle Engine during Throttling

Min Chen, Jiyuan Zhang, and Hailong Tang

School of Energy and Power Engineering, Beihang University, Beijing 100191, China

Correspondence should be addressed to Hailong Tang; 75249612@qq.com

Received 20 November 2017; Revised 17 March 2018; Accepted 2 April 2018; Published 22 April 2018

Academic Editor: Konstantinos Kyprianidis

One advantage of the adaptive cycle engine (ACE) is its ability of throttling with constant airflow by the combined control of variable geometries, resulting in an improvement of spillage drag. However, the improvement is achieved at risk of a complex technical solution and control. This article investigates the selection scheme of variable geometries and engine configuration. It focuses on the performance of a three-stream ACE during throttling, whose configuration and control schedule are simpler than other types of ACEs. Five variable geometries are selected from seven available options through comparison analysis. The uninstalled thrust decreases from 100% to 60.36% during the subsonic throttling and to 59.81% during the supersonic throttling. Benefitting from the decreased spillage drag, the installed performance of the three-stream ACE is improved to some degree during throttling. This improvement is less than the result of a three-bypass ACE, whose configuration and control schedule are more complex. Thus, the three-stream ACE is a compromise design considering the technical risk and variable cycle characteristic, which is a better platform to verify the component technology and control schedule for the further research on a more complex type of ACE.

1. Introduction

With the development of electronic technique and missile performance, the mission requirement of aircraft has changed a lot. The design objectives of next-generation aircraft include beyond-the-horizon campaign, short take-off and vertical landing, wider flight envelope and combat radius [1]. These design objectives affect the requirement of aircraft engine design. On the one hand, the engine should have the turbojet features, such as higher specific thrust, to realize non-augmented supersonic cruising and high subsonic climbing. On the other hand, it should also have the turbofan feature, such as lower specific fuel consumption (SFC), to accomplish long-range reconnaissance [2–5]. With the development of aeroengine technology in the last 80 years, the thrust/weight ratio and SFC have improved a lot [6]. However, none of the traditional engine types (turbojet and turbofan) can meet all mission requirements mentioned above. Therefore, a new type of engine should be introduced to achieve those conflicting goals, which led to the studies of variable cycle engine (VCE) [7–9] and some other innovative engine types [10, 11].

In the last 50 years, many aeroengine companies, colleges, and research centers have conducted investigations of several types of VCE, including three spool modulating bypass ratio VCE [9], double bypass VCE [12], selective bleed VCE [13], and variable stream control engine [14]. These studies involved the general structure and performance analysis, optimization of cycle parameters, variable geometry control schedule [15–17], and so on. According to these studies, one advantage of the VCE over traditional engine types is its potential in keeping airflow constant during the cruise throttling, which can obviously decrease the spillage drag and improve the installed performance. The turbine inlet temperature of military aircraft engine is increased to improve the supersonic performance. The increased turbine inlet temperature also increases the thrust level. For the traditional military aircraft engine, when it throttles from high thrust level back to cruise power settings, it has to reduce the airflow, resulting in increased spillage drag losses [7, 8]. In that case, compared with traditional engine, the VCE can generate equal installed thrust with less fuel consumption, resulting in the improvement of installed SFC and the increase of cruise

range. Keeping the airflow constant during the supersonic cruising can also reduce the risk of inlet supersonic buzz, which is caused by the inlet-engine airflow mismatch.

As a new concept of VCE, the adaptive cycle engine (ACE) is developed based on the double bypass VCE. It is an important part of the US Department of Defense's Adaptive Versatile Engine Technology (ADVENT) and the Adaptive Engine Technology Development (AETD) programs [18–20]. The typical type of ACE consists of a third bypass duct and more variable geometries than the VCE [2, 3, 21, 22]. Due to the additional bypass duct and variable geometries, the ACE can modulate the airflow and pressure ratio in a wider range than the VCE. However, it also makes the control schedule of the ACE more complicated, which is worthy of further investigation.

Lyu et al. [3] and Lyu [4] conducted a study on combined variable geometry control of an ACE during throttling based on matching mechanism, obtaining a proper control schedule to maintain the airflow during throttling and improve installed performance of the ACE. This research involved six variable geometries, but it did not explain the selection scheme of variable geometries. Although the introduction of extensive variable geometries enhances the modulation's flexibility of airflow and thrust, it can increase the complexity of the engine's configuration and control schedule, resulting in high technical risk [23–26]. For example, the nozzle area of the high-pressure turbine (HPT) guide vane is an important parameter of the engine, which affects the operating line of the compressor and the operational flexibility of the engine. However, the entry temperature of the HPT guide vane is extremely high, which makes it risky to install variable geometries. Therefore, it is desirable to study the necessity of installing variable geometries into the HPT guide vane. What is more, the typical configuration of the ACE is a three-bypass engine, which is difficult to be derived from the existing versatile gas turbine engines. There are several components with innovative technologies, and related control systems should be researched before the further design of the three-bypass ACE. Therefore, it is necessary to design an ACE with simpler configuration as the platform for the researches and tests of the components and control system at first.

Due to the motivation mentioned above, this article studies the throttle performance of a three-stream ACE. The configuration of the three-stream ACE is shown in Figure 1. It is a simple type of ACE and has only two bypass ducts, less than the typical ACE. The main components of the ACE are demonstrated in Figure 2. The fan system of this ACE is divided into two parts, including the front fan stage (FFAN) and rear fan stage (RFAN). Both the FFAN and RFAN are driven by the low-pressure turbine (LPT). The high-pressure compressor (HPC) is driven by the HPT. The nozzle system of this ACE consists of two parts, including the main nozzle and the bypass nozzle. The airflow from the first bypass duct mixes with the gas from the core engine at the variable area bypass injector (VABI). As shown in these figures, the three-stream ACE is similar with the turbofan. It can be regarded as a mixed turbofan equipped with a front fan stage and an outer bypass duct. Therefore, it is easier to be derived from the existing versatile turbofans than the other types of ACE.

The aim of this article is to study the matching mechanism of the variable geometries of this ACE, keep enough potential in maintaining airflow during throttling with fewer variable geometries, and analyze the effect of its simple configuration on its variable cycle characteristic. The available variable geometries of this ACE are shown in Figure 3. It consists of the variable stator vane of RFAN (VSV_{RFAN}) and HPC (VSV_{HPC}), the variable area nozzle of the HPT guide vane (VAN_{HPT}) and LPT guide vane (VAN_{LPT}), VABI and the variable area section of the main nozzle's throat (A_8), and the bypass nozzle's exit (A_{28}). This article analyzes each variable geometry's effects on ACE's performance through the sensitivity analysis. Then, the necessary variable geometries are selected based on the comparison of its effect on ACE's performance and the technical risk. The installed performance during the cruise throttling with constant airflow can be obtained through the combined control of the selected variable geometries. Then, the improvement of installed performance during throttling with constant airflow can be obtained, compared with the result of throttling by reducing the airflow with declined low-pressure rotor speed (LPRS). Finally, compared with the result of the three-bypass ACE discussed in literature [3, 4], the influence of three-stream ACE's simple configuration and control schedule on its variable cycle characteristic can be demonstrated. The result shows that the three-stream ACE is a compromise design considering the technical risk and variable cycle characteristic.

In this paper, Introduction introduces the background and the motivation of this research. The next section gives a brief description on ACE's structure and the performance model applied in this research. Section 3 discusses the selection scheme of the variable geometries based on sensitivity analysis. Section 4 presents the installed performance improvement of three-stream ACE and compares it with the result of three-bypass ACE. The final section draws the conclusions.

2. Structure Analysis and Performance Model of ACE

2.1. Structure Analysis. As Figure 1 shows, the three-stream ACE is a two-bypass turbine engine. Distinct from the other types of ACE, it has only one operating mode. When it operates at this mode, all bypass ducts are open. The flow path of it is shown in Figure 4. The airflow from the FFAN passes through the RFAN and the second bypass duct. The airflow from the RFAN passes through the first bypass duct and the core engine. Then, the gas from the LPT mixes with the air from the first bypass duct at the VABI and will be exhausted through the main nozzle. The second bypass airflow is exhausted through the bypass nozzle.

The structure figure of the three-bypass ACE is shown in Figure 5. Different from three-stream ACE, it has the third bypass duct, front VABI, and the core-driven fan stage (CDFS) [3]. The three-bypass ACE has two operating modes: double bypass mode and triple bypass mode. When the

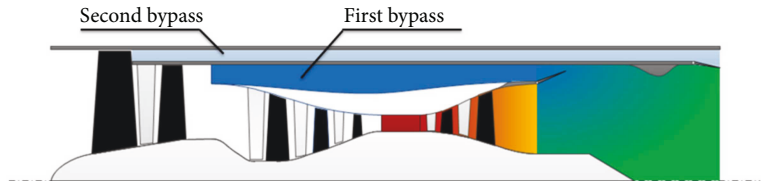

Figure 1: The configuration of three-stream ACE.

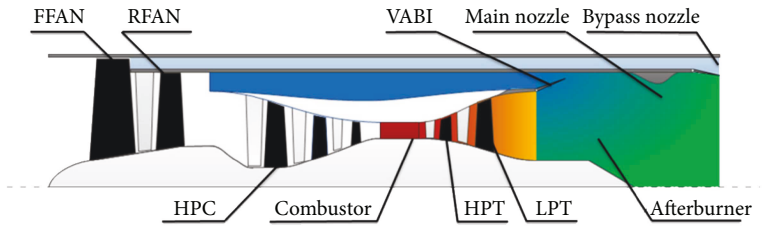

Figure 2: The main components of three-stream ACE.

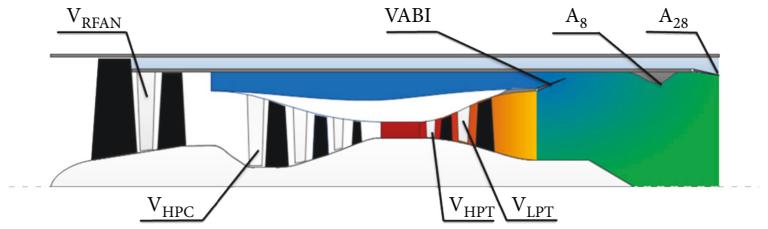

Figure 3: The available variable geometries of three-stream ACE.

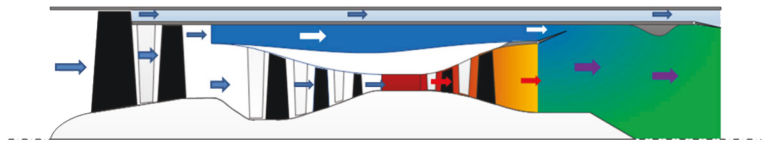

Figure 4: Flow path figure of three-stream ACE.

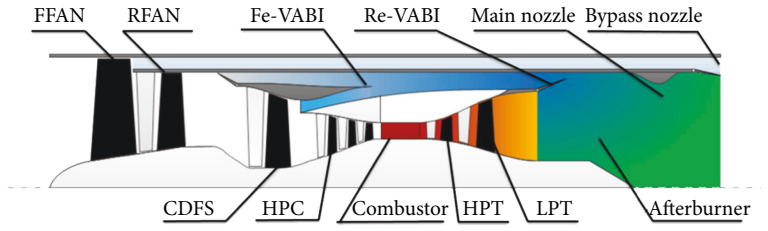

Figure 5: Structure figure of three-bypass ACE.

three-bypass ACE operates at double bypass mode, all of the airflow from the RFAN passes through the CDFS, which is the high-power mode of the CDFS. When it operates at triple bypass mode, part of the airflow from the RFAN passes through the second bypass duct, which is the part-power mode of the CDFS. To maintain the performance of the three-bypass ACE, the CDFS is supposed to operate efficiently within a wide range of power. Therefore, the CDFS is a critical component of the three-bypass ACE and one of the greatest challenges during the design stage [24, 25]. More details about the operating principle and structure analysis can be obtained in the literature [3].

2.2. Performance Model. The performance model developed in this article is a zero-dimensional (0D) engine model. It is convenient to develop parametric cycle analysis, overall performance analysis, and control schedule analysis based on this model [2]. It consists of several component calculation

modules, including all the components shown in Figure 2. The component characteristic parameter is given in the form of a characteristic map or empirical formulas. For the variable geometries, such as VSV_{RFAN}, their characteristic parameters are related with the geometry parameters. Given the thermodynamic parameters of gas at the components' inlet section, parameters of gas at its exit section will be calculated, including mass flow, velocity, temperature, and pressure. These component calculation modules are connected together according to their thermodynamic and mechanical relationship and make up the ACE's performance model. The losses in the bypass ducts are considered in the form of total pressure recovery coefficients. The factors affecting gas property, such as ambient temperature, ambient humidity, and gas ingredients, are taken into consideration in this model. The model also considers the mixing loss of the VABI, the effects of bleed air, the shaft power set aside for aircraft, and so on [2].

The performance model has two major functions: design point calculation and off-design point calculation. Design point calculation is the base of the other, since the key geometry parameters of ACE are determined in this process. To complete the design point calculation, some important design parameters should be given in advance, including altitude, Mach number, total pressure ratio, airflow at the inlet, and split ratio. Based on the result of design point calculation and the given operating condition, the off-design point performance can be obtained. The essence of off-design point calculation is deriving the components' operating points, which is determined by the components they coupled with. It is a highly iterative process and requires successive "guesses" of the operating points on components' characteristic maps, which is represented by the matching guesses. These matching guesses are updated until the matching constraints are satisfied [27]. The matching constraints include flow compatibility of the HPT and LPT, power equilibrium of the high-pressure rotor (HPR) and low-pressure rotor (LPR), static pressure equilibrium of the VABI, and compatibility of A_8 and A_{28}. Given the operating conditions of the ACE, including the altitude, Mach number, and the control schedule, the number of matching guesses equals to the number of matching constraints. In that case, the matching guesses can be calculated through the multidimensional Newton–Raphson iteration method. Then, the components' operating points are determined by the matching guesses and ACE's overall performance can be calculated easily. More details about the 0D engine performance model can be obtained in the literature [2, 28, 29]. The arithmetic of this performance model has been tested and verified accurately in many projects [30, 31].

The design point of ACE is set as sea level static condition (SLS), which is the take-off condition. Some of the important design parameters are shown in Table 1. The value of these design parameters is determined according to the development trend of the next 10 years and the requirement of specific thrust and SFC.

W_a is the total airflow of the ACE, T_{t4} is the HPT inlet total temperature, π_t is the total compression ratio, π_{FAN} is the compression ratio of the fan stage, π_{FFAN} is the compression ratio of FFAN, π_{RFAN} is the compression ratio of RFAN, π_{HPC} is the compression ratio of HPC, D_F is the diameter of the engine at fan entry, B_t is the total bypass ratio, B_1 is the first bypass split ratio and B_2 is the second bypass split ratio, and N_1 is the relative rotating speed of LPR. The fan stage of three-stream ACE consists of the FFAN and RFAN. The definition of the fan stage compression ratio, bypass ratio, and split ratio is expressed in (1).

Table 1: Design parameters of three-stream ACE.

Parameter	W_a (kg/s)	T_{t4} (K)	D_F (m)	B_t	B_1	B_2
Value	165	1750	1.052	1.0125	0.4375	0.4
Parameter	π_t	π_{FAN}	π_{FFAN}	π_{RFAN}	π_{HPC}	N_1
Value	32	3.404	1.84	1.85	9.40	100%

$$\begin{aligned} \pi_{FAN} &= \pi_{FFAN} \times \pi_{RFAN}, \\ B_t &= \frac{(W_{aFB} + W_{aSB})}{W_{aHPC}}, \\ B_1 &= \frac{W_{aFB}}{W_{aHPC}}, \\ B_2 &= \frac{W_{aSB}}{W_{aRFAN}}, \end{aligned} \tag{1}$$

where W_{aFB} is the airflow of the first bypass duct, W_{aSB} is the airflow of the second bypass duct, W_{aRFAN} is the airflow of the RFAN, and W_{aHPC} is the airflow of the HPC.

Through the design point calculation, the key geometry parameters of the ACE and the performance of the ACE at the design point can be calculated. Given the control schedule and operating condition, the performance of the ACE at off-design point can be obtained. The investigation of the selection scheme of variable geometries can be developed through this model.

3. Selection Scheme Analysis of Variable Geometries

In this article, the performance during supersonic cruise throttling (11 km, 1.5 Ma) and subsonic cruise throttling (11 km, 0.8 Ma) is researched. The selection scheme of variable geometries should be determined before the investigation of combined control schedule. The selection scheme is designed to obtain enough potential in maintaining airflow during throttling with fewer variable geometries. All of the seven available variable geometries mentioned in Figure 3 are taken into consideration. The effects of each variable geometry are analyzed through sensitivity analysis. Then, five of them are finally selected based on the comparison of their effects on ACE's performance and technical risk. Both the subsonic cruise condition and supersonic cruise condition are taken into consideration. To maintain the airflow during throttling, the control schedule of ACE is set as keeping LPRS constant. The analysis described in Section 3 is all about uninstalled performance, which is the base for the investigation of installed performance.

3.1. Sensitivity Analysis of Variable Geometries. Sensitivity analysis is one of the control variable analysis methods, which essentially is a single-variable analysis method. During this analysis process, seven variable geometries are adjusted, respectively. When one of the variable geometries is adjusted, the others are kept unchanged. The origin value and adjusted value of variable geometries are shown in Table 2.

The value of VSV_{RFAN} and VSV_{HPC} represents the actual degree of the stator vane. The value of other variable geometries represents the coefficient of area, which is the ratio of the set area to the designed area. The definition of the coefficient of area is shown in (2). According to Table 2, VSV_{RFAN} and VSV_{HPC} are turned up at 5°, respectively, and the coefficients of other variable geometries' area are turned down at 10%, respectively, during the sensitivity analysis.

$$R_A = \frac{A_{\text{Set}}}{A_{\text{Designed}}}, \tag{2}$$

where R_A is the coefficient of area, A_{Set} is the set area, and A_{Designed} is the designed area. The change in ACE's performance is expressed by the relative change rate, whose definition is shown in (3).

$$D_P = \frac{V_{\text{Adjusted}} - V_{\text{Original}}}{V_{\text{Original}}}, \tag{3}$$

where D_{P} is the relative change rate of the ACE performance, V_{Adjusted} is the adjusted value, and V_{Original} is the original value. The sensitivity analysis results of VSV_{RFAN}, VSV_{HPC}, VAN_{HPT}, and VAN_{LPT} are shown in Figures 6–8. The results of other variable geometries are shown in Figures 9–11. There are five important performance parameters shown in these figures, including thrust, airflow, and surge margin of the FFAN (SM_{FFAN}), RFAN (SM_{RFAN}), and HPC (SM_{HPC}).

When the ACE operates at the subsonic cruise or supersonic cruise condition, turning up VSV_{RFAN} increases the thrust and airflow. This result can be explained through the matching mechanism analysis. Directly, turning up VSV_{RFAN} increases the flow capacity of RFAN, resulting in the decrease in pressure behind FFAN and the improvement of the surge margin of FFAN. As a result, the corrected flow of FFAN increases as the engine airflow increase. On the other hand, the increase in engine airflow increases the compression work of the LPR, resulting in the decrease in LPRS. To keep the LPRS constant, fuel flow has to increase, resulting in the increase in T_{t4} and thrust.

When the ACE operates at the subsonic cruise or supersonic cruise condition, turning up VSV_{HPC} increases the thrust and decreases airflow. Directly, turning up VSV_{HPC} increases the flow capacity of the HPC, resulting in the increase in the compression work of the HPC. The HPRS drops because of the deficiency of HPT's output work. The decreased HPRS leads to the decrease in the rotating speed ratio (RSR), which is the ratio of HPRS to LPRS, resulting in the decrease in SM_{FFAN} and $SM_{RFAN.}$ The definition of RSR is shown in (4). The operating point of FFAN moves up along its referred speed line, causing the decrease in engine airflow. Under the comprehensive influence of VSV_{HPC} and HPRS, the core flow tends to drop, resulting in the decrease in LPT's output work. As a result, the LPRS tends to drop. To keep the LPRS constant, fuel flow has to increase, resulting in the increase in T_{t4} and thrust.

$$\text{RSR} = \frac{\text{HPRS}}{\text{LPRS}}. \tag{4}$$

When the ACE operates at the subsonic cruise or supersonic cruise condition, turning down VAN_{HPT} increases the thrust and decreases airflow. Directly, turning down VAN_{HPT} increases the HPT's expansion ratio, leading to the increase in HPT's output work and decrease in LPT's inlet total temperature (T_{t5}). Excess HPT's output work causes the increase in HPRS while the decrease in T_{t5} leads to the decrease in LPT's output work, resulting in the decrease in LPRS. To keep the LPRS constant, fuel flow has to increase, resulting in the increase in T_{t4} and thrust. Under the comprehensive influence of VAN_{HPT} and T_{t4}, the core flow almost keeps constant. The constant core flow and rising HPRS lead to the obvious decrease in SM_{HPC}.

When the ACE operates at the subsonic cruise or supersonic cruise condition, turning down VAN_{LPT} increases the thrust and decreases airflow. Directly, turning down VAN_{LPT} leads to the decrease in HPT's expansion ratio and increase in the LPT's expansion ratio. The decrease in HPT's expansion ratio leads to the decrease in HPT's output work, resulting in the decrease of the HPRS and core flow. Under the comprehensive influence of decreased core flow and increased LPT's expansion ratio, the LPT's output work tends to decrease, resulting in the decrease of the LPRS. To keep the LPRS constant, fuel flow has to increase, resulting in the increase in T_{t4} and thrust. The decreased HPRS and increased T_{t4} lead to the obvious decrease in SM_{HPC}. The decrease of the HPRS also leads to the decrease in HPC's flow capacity, resulting in the increase in RFAN's back pressure. Then, RFAN's surge margin and flow capacity decrease, leading to the decrease in FFAN's corrected airflow and engine airflow.

When the ACE operates at the subsonic cruise or supersonic cruise condition, turning down the VABI decreases the thrust and airflow. Directly, turning down the VABI leads to the increase in LPT's expansion ratio, resulting in the increase in LPT's output work. The LPRS tends to rise due to the excess LPT's output work. To keep the LPRS constant, fuel flow has to decrease, resulting in the decrease in T_{t4} and thrust. On the other hand, turning down the VABI causes the increase in RFAN's back pressure, leading to the decrease in RFAN's surge margin and flow capacity. The decreased RFAN's flow capacity leads to the increase in FFAN's back pressure. As a result, FFAN's operating point moves up along the referred speed line, resulting in the decrease in airflow.

When the ACE operates at the subsonic cruise or supersonic cruise condition, turning down A_8 increases the thrust and decreases the airflow. Directly, turning down A_8 decreases LPT's expansion ratio, leading to the decrease in LPT's output work. The LPRS tends to drop due to the deficiency of LPT's output work. To keep the LPRS constant, fuel flow has to increase, resulting in the increase in T_{t4} and thrust. On the other hand, the decrease in A_8 leads to the

Table 2: Adjustment of variable geometries during sensitivity analysis.

	VSV_{RFAN}	VSV_{HPC}	VAN_{HPT}	VAN_{LPT}	VABI	A_8	A_{28}
Original	−30°	−20°	1	1	1	1	1
Adjusted	−25°	−15°	0.9	0.9	0.9	0.9	0.9

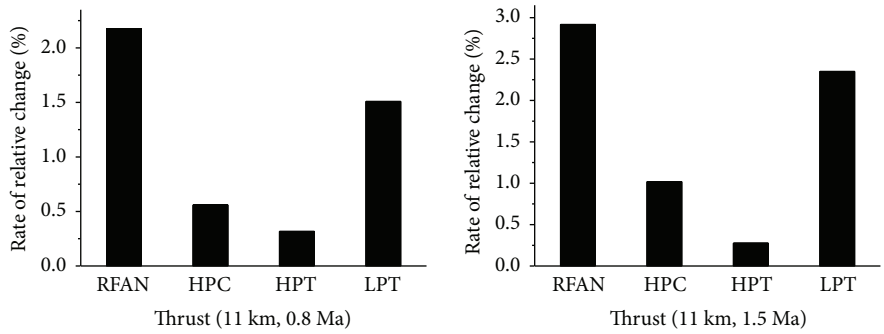

Figure 6: Sensitivity analysis of variable geometries on thrust (part 1).

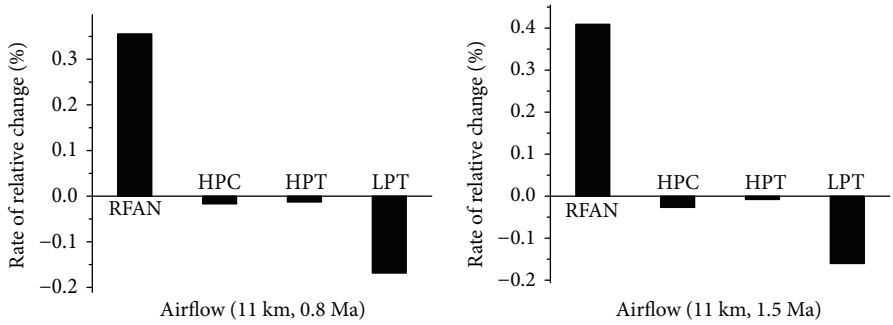

Figure 7: Sensitivity analysis of variable geometries on airflow (part 1).

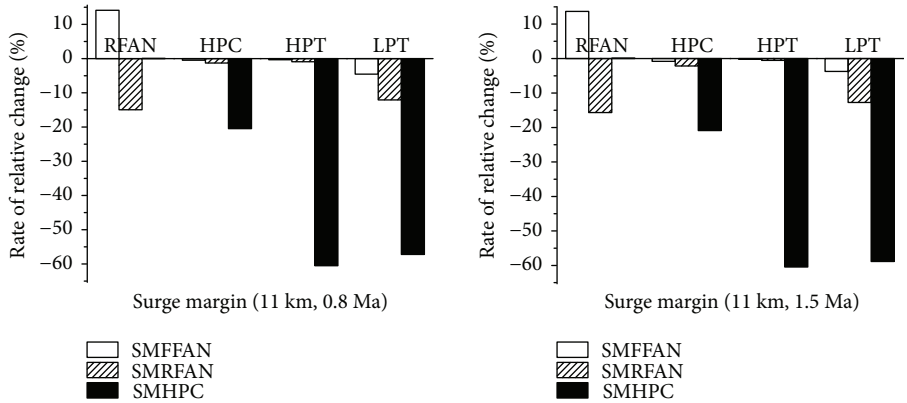

Figure 8: Sensitivity analysis of variable geometries on surge margin (part 1).

increase in RFAN's back pressure, causing the decrease in RFAN's surge margin and flow capacity. The decreased RFAN's flow capacity leads to the increase in FFAN's back pressure. As a result, FFAN's operating point moves up along the referred speed line, resulting in the decrease in airflow.

When the ACE operates at the subsonic cruise or supersonic cruise condition, turning down A_{28} increases the thrust and decreases the airflow. Directly, turning down A_{28} increases the back pressure of FFAN, resulting in the decrease in airflow and FFAN's surge margin. On the other

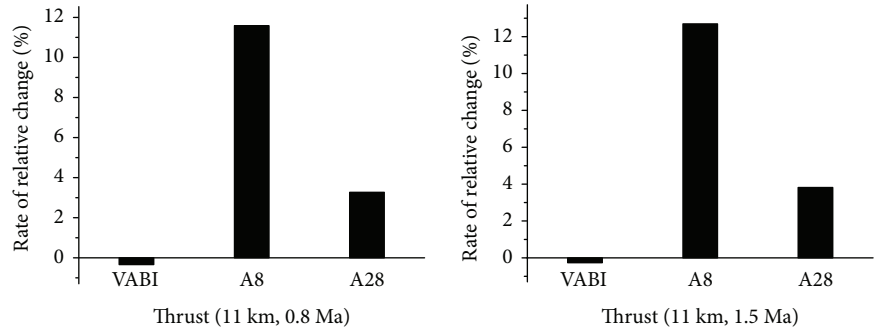

Figure 9: Sensitivity analysis of variable geometries on thrust (part 2).

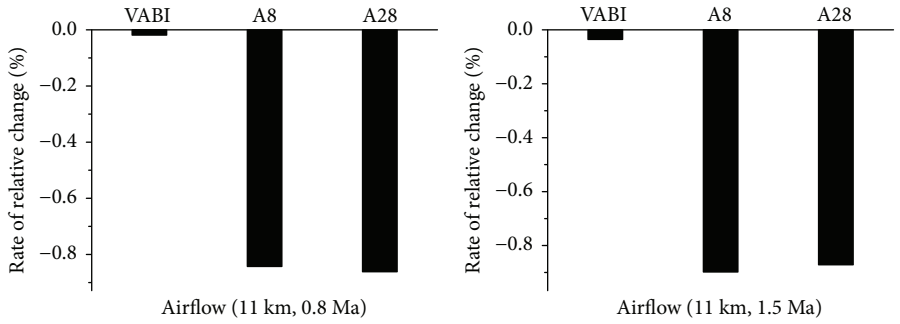

Figure 10: Sensitivity analysis of variable geometries on airflow (part 2).

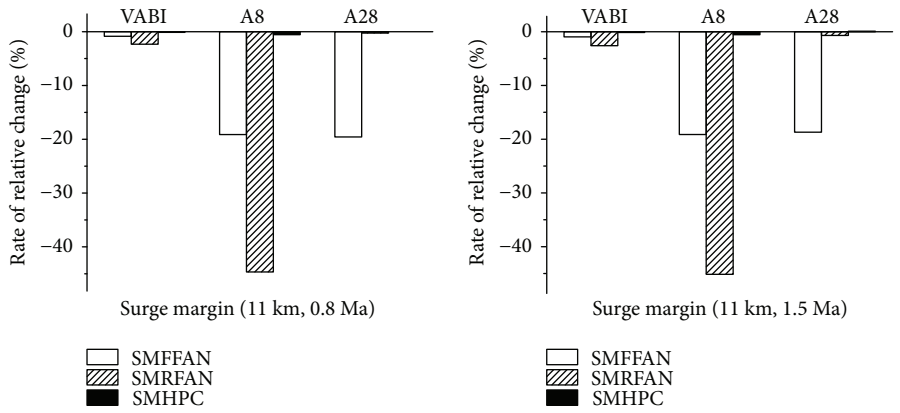

Figure 11: Sensitivity analysis of variable geometries on surge margin (part 2).

hand, turning down A_{28} causes more air flow through RFAN, leading to the increase in LPR's compression work. The LPRS tends to drop due to the deficiency of LPT's output work. To keep the LPRS constant, fuel flow has to increase, resulting in the increase in T_{t4} and thrust.

3.2. Selection Scheme Analysis. To compare the effect of variable geometries' adjustment on ACE's performance conveniently, the result of sensitivity analysis is summarized in Table 3. In this table, the sign "+" indicates that adjusting the variable geometry in this way can cause the increase in the corresponding performance parameter, while "−" indicates the opposite effect and "/" indicates that there is no measurable effect. More "+" or "−" indicates a more obvious effect.

Although the introduction of extensive variable geometries enhances the ACE modulation's flexibility of airflow and thrust, it can also increase the complexity of configuration and control schedule. One rational solution is to select as few variable geometries as possible to achieve enough potential in modulating airflow and thrust. The major objective of variable geometries' combined control is keeping the airflow constant as the thrust drops.

The selection scheme is determined through several combined control analyses. At first, only the variable geometries with great effect on the ACE thrust will be selected. Based on the sensitivity analysis results shown in Table 3, the combined control schedule of these variable geometries can be designed to modulate thrust with constant airflow. The

Table 3: Result of variable geometries' sensitivity analysis.

	VSV_{RFAN} +5°	VSV_{HPC} +5°	VAN_{HPT} −10%	VAN_{LPT} −10%	VABI −10%	A_8 −10%	A_{28} −10%
Thrust	++	+	+	++	−	+++	++
Airflow	++	−	−	− −	−	− − −	− − −
SM_{FFAN}	+++	−	−	− −	−	− − −	− − −
SM_{RFAN}	− −	−	−	− −	−	− − −	/
SM_{HPC}	/	− −	− − −	− − −	/	−	/

variation range of the thrust will be limited by several constraints, such as components' surge margin and efficiency. To ensure that the engine can operate safely, there are lower bounds for the components' surge margin taken into account. To avoid the deterioration of SFC, there are lower bounds for the components' efficiency taken into consideration. In order to achieve a wider variation range of thrust, other variable geometries should be added. Finally, through comparing the available variation range of thrust with the technical risk, the selection scheme of variable geometries will be determined.

Firstly, considering A_8 and VSV_{RFAN} have an obvious effect on the thrust and an opposite effect on the airflow, they are selected as the first group to control the throttling process while others are kept unchanged. Through turning up A_8 and turning down VSV_{RFAN}, the airflow can be kept constant as the thrust reduces. The control schedule of variable geometries is shown in Table 4. Through the combined control of variable geometries in group 1, the thrust decreases from 100% to 83.19% during subsonic cruise and to 82.53% during supersonic cruise with constant airflow. The variation range of thrust is limited by several constraints, which are shown in Table 5, where R_F denotes the relative change rate of thrust, "η_{FFAN}" denotes the efficiency of FFAN, "η_{RFAN}" denotes the efficiency of RFAN, "η_{HPC}" denotes the efficiency of the HPC, "✓" denotes this constraint is satisfied, and "★" denotes this constraint limits the variation range of thrust. The result shows that η_{FFAN} limits the upper bound of the thrust and airflow limits the lower bound of the thrust. If A_8 and VSV_{RFAN} are adjusted to increase the thrust further, η_{FFAN} will drop beyond the lower bounds. If A_8 and VSV_{RFAN} are adjusted to decrease the thrust further, the airflow cannot be kept constant. Therefore, additional variable geometries should be selected to broaden the variation range of thrust.

Based on the analysis above, the variable geometry with great effect on the airflow and η_{FFAN} should be selected to modulate thrust with constant airflow, combined with A_8 and VSV_{RFAN}. Considering A_{28} has a great effect on the airflow and SM_{FFAN} (which is directly related to η_{FFAN}) and has almost no effect on other components, it is selected as the addition for the first group of variable geometries. The control schedule of this group of variable geometries is shown in Table 6. Through turning down A_8 and turning up VSV_{RFAN} further, the thrust rises but η_{FFAN} tends to drop beyond the lower bound. In that case, turning down A_{28} can improve η_{FFAN} at the cost of SM_{FFAN} and increase the thrust further. Through turning up A_8 and turning down VSV_{RFAN} further, the thrust drops but the airflow tends to drop too. In that case, turning up A_{28} can keep the airflow constant and decrease the thrust further. Consequently, the addition of A_{28} broadens the variation range of the thrust with constant airflow. Through the combined control of variable geometries in group 2, the thrust decreases from 100% to 67.77% during subsonic cruise and to 65.29% during supersonic cruise with constant airflow. However, if the variable geometries are adjusted to modulate the thrust in a wider range, SM_{RFAN} and η_{RFAN} tend to drop beyond the lower bound, as shown in Table 7. Therefore, additional variable geometries should be selected to broaden the variation range of thrust.

Based on the analysis above, VAN_{LPT} should be selected as the addition for the second group, considering its great effect on SM_{RFAN} and η_{RFAN}. However, VAN_{LPT} also has a great effect on η_{HPC} and SM_{HPC}, which is different from the other variable geometries in the second group. In order to fulfill the potential of VAN_{LPT}, additional variable geometry with a great effect on η_{HPC} and SM_{HPC} should be selected. As a result, VAN_{LPT} and VSV_{HPC} are selected together as the addition for the second group. The control schedule of this third group of variable geometries is shown in Table 8. Through turning down A_8 and A_{28} and turning up VSV_{RFAN} further, the thrust rises but the SM_{RFAN} tends to drop beyond the lower bound. In that case, turning up VAN_{LPT} can improve SM_{RFAN} at the cost of η_{HPC}, which can be compensated by turning up VSV_{HPC}. Through turning up A_8 and A_{28} and turning down VSV_{RFAN} further, the thrust drops but η_{RFAN} tends to drop beyond the lower bound. In that case, turning down VAN_{LPT} can improve the SM_{RFAN} at the cost of η_{HPC}, which can be compensated by turning down VSV_{HPC}. Consequently, the addition of VAN_{LPT} and VSV_{HPC} broadens the variation range of the thrust with constant airflow. Through the combined control of variable geometries in group 3, the thrust decreases from 100% to 60.36% during subsonic cruise and to 59.81% during supersonic cruise with constant airflow.

As for the VABI, it has almost no effect on ACE's thrust, airflow, and the operating point of component, compared with other variable geometries. Therefore, it is unnecessary to introduce variable geometries into it. As for VAN_{HPT}, it has a great effect on SM_{HPC}, which is similar with VAN_{LPT}. However, compared with VAN_{LPT}, it has almost no effect on thrust, airflow, and other components except the HPC. Thus, its effect on modulating throttling can be replaced by

Table 4: Control schedule of variable geometries (group 1).

	R_F	VSV_{RFAN}	VSV_{HPC}	VAN_{HPT}	VAN_{LPT}	VABI	A_8	A_{28}
Subsonic	100%	−7°	−20°	1.0	1.0	1.0	0.95	1.0
	83.19%	−22°	−20°	1.0	1.0	1.0	1.06	1.0
Supersonic	100%	−5°	−20°	1.0	1.0	1.0	0.95	1.0
	82.53%	−20°	−20°	1.0	1.0	1.0	1.06	1.0

Table 5: Important parameter during throttling (group 1).

	R_F	Airflow	SM_{FFAN}	SM_{RFAN}	SM_{HPC}	η_{FFAN}	η_{RFAN}	η_{HPC}
Subsonic	100%	✓	✓	✓	✓	★	✓	✓
	83.19%	★	✓	✓	✓	✓	✓	✓
Supersonic	100%	✓	✓	✓	✓	★	✓	✓
	82.53%	★	✓	✓	✓	✓	✓	✓

Table 6: Control schedule of variable geometries (group 2).

	R_F	VSV_{RFAN}	VSV_{HPC}	VAN_{HPT}	VAN_{LPT}	VABI	A_8	A_{28}
Subsonic	100%	0°	−20°	1.0	1.0	1.0	0.95	0.8
	67.77%	−30°	−20°	1.0	1.0	1.0	1.09	1.1
Supersonic	100%	0°	−20°	1.0	1.0	1.0	0.95	0.8
	65.29%	−30°	−20°	1.0	1.0	1.0	1.08	1.15

Table 7: Important parameter during throttling (group 2).

	R_F	Airflow	SM_{FFAN}	SM_{RFAN}	SM_{HPC}	η_{FFAN}	η_{RFAN}	η_{HPC}
Subsonic	100%	✓	✓	★	✓	✓	✓	✓
	67.77%	✓	✓	✓	✓	✓	★	✓
Supersonic	100%	✓	✓	★	✓	✓	✓	✓
	65.29%	✓	✓	✓	✓	✓	★	✓

Table 8: Control schedule of variable geometries (group 3).

	R_F	VSV_{RFAN}	VSV_{HPC}	VAN_{HPT}	VAN_{LPT}	VABI	A_8	A_{28}
Subsonic	100%	0°	0°	1.0	1.1	1.0	0.95	0.8
	60.36%	−30°	−20°	1.0	0.92	1.0	1.1	1.2
Supersonic	100%	0°	0°	1.0	1.1	1.0	0.95	0.8
	59.81%	−30°	−20°	1.0	0.95	1.0	1.08	1.15

VAN_{LPT}. What is more, the guide vane of HPT operates at an extremely high temperature and needs a complex cooling system to maintain its safety and durability. In that case, installing variable geometries into it is a great challenge to the reliability and feasibility of the system. Therefore, it is unnecessary to introduce variable geometries into the guide vane of HPT. Finally, five variable geometries are selected from the seven available choices through comparison of their effects on modulating throttling and the technical risk. Through the combined control of these five variable geometries, including VSV_{RFAN}, VSV_{HPC}, VAN_{LPT}, A_8, and A_{28}, the thrust can be modulated in a wide range with constant airflow. The improvement of ACE's installed performance during cruise throttling will be discussed in Section 4.

4. Installed Performance Improvement of ACE

For the mixed mission aircraft, cruise throttling is an important operating condition. For the type of engine lack of variable geometries, such as traditional turbofan and turbojet, it has to reduce the airflow to decrease the thrust, which can incur large spill drag losses and obvious deterioration in

installed SFC. One advantage of the ACE over traditional types of engine is its potential in maintaining airflow during the cruise throttling through the combined control of variable geometries. Firstly, through the combined control of five variable geometries selected in Section 3, the three-stream ACE can keep airflow constant during the subsonic cruise throttling and supersonic cruise throttling. Secondly, compared with the installed performance during cruise throttling modulated by reducing airflow, the improvement of installed performance achieved by maintaining airflow during cruise throttling can be obtained. Finally, through the comparison of the installed performance improvement of the three-stream ACE and the three-bypass ACE, the influence of the three-stream ACE's simple configuration and control schedule on its variable cycle characteristic can be analyzed.

When the installed performance of the three-bypass ACE was discussed in literature [4], it only focused on the improvement achieved by reducing spillage drag. To compare the installed performance of these two types of ACE, this article only focuses on the spillage drag and does not take the nozzle boattail drag, weight, and other factors into consideration. The installed performance is calculated based on the inlet characteristic maps. At first, the inlet capture area can be calculated according to its operating design point. When the operating condition of the ACE is given, the uninstalled performance can be calculated through the performance model introduced in Section 2.2. Then, the inlet airflow coefficient and pressure recovery coefficient can be obtained through iterative calculations. After that, the inlet spillage drag coefficient can be obtained, which takes the inlet nacelle pressure drag and inlet incremental drag into consideration. Then, the uninstalled performance of the ACE can be corrected according to the pressure recovery coefficient, nozzle expansion ratio, inlet spillage drag coefficient, and so on. Finally, the installed performance of the ACE can be obtained. The calculation flowchart is shown in Figure 12. More details about the inlet characteristic maps and the installed performance calculation can be obtained in the literature [32, 33–35]. In this article, the inlet operating design point is set as 11 km, 1.0 Ma.

To make the description simply, the cruise throttling with constant airflow is denoted as "constant-airflow throttling" and the cruise throttling modulated by reducing airflow is denoted as "reduced-airflow throttling."

4.1. Improvement of Installed Performance of Three-Stream ACE. Based on the analysis in Section 3, the airflow can be kept constant during the cruise throttling by turning up A_8 and A_{28} and turning down VSV_{RFAN}, VSV_{HPC}, and VAN_{LPT}, which is shown in Figures 13 and 14. The unit of thrust is daN, which stands for 10 N. The definition of coefficient of area is shown in (2).

Some important performance parameters of the ACE during the constant-airflow throttling are shown in Table 9, where $W_{a\mathrm{FFAN}}$ is the airflow of the FFAN, $W_{a\mathrm{RFAN}}$ is the airflow of RFAN, $W_{a\mathrm{HPC}}$ is the airflow of the HPC, V_{28} is the bypass nozzle jet velocity, and V_9 is the main nozzle jet velocity. The nozzle jet velocity is the absolute value of relative velocity between exhausted gas and the engine. The max jet velocity of bypass nozzle is acoustic velocity, because the bypass nozzle is a type of convergent nozzle. Therefore, the bypass nozzle jet velocity is less than the flight velocity during the supersonic cruise. On the other hand, the static pressure of the second bypass exhausted air is higher than the atmospheric pressure due to the compression of FFAN. Under the comprehensive influence of flight velocity, jet velocity, and the pressure differentials between exhausted air and atmosphere, the bypass nozzle can still generate thrust.

In order to calculate the installed performance during reduced-airflow throttling, the variable geometries are kept constant as the initial value of constant-airflow throttling and the LPRS is reduced to decrease the airflow. In order to compare the installed performance during constant-airflow throttling and reduced-airflow throttling, their variation ranges of uninstalled thrust are set as the same value. The comparison of the airflow during throttling is shown in Figure 15. The definition of relative installed airflow (R_{airflow}) is shown in (5), where $W_{a,\mathrm{actual}}$ is the actual installed airflow and $W_{a,\mathrm{initial}}$ is the initial installed airflow during throttling.

$$R_{\mathrm{airflow}} = \frac{W_{a,\mathrm{actual}}}{W_{a,\mathrm{initial}}}. \tag{5}$$

The result shows that through the combined control of the five variable geometries, the airflow can be kept constant during the constant-airflow throttling. However, the airflow decreases from 100% to 81.6% during the subsonic reduced-airflow throttling and to 81.1% during the supersonic reduced-airflow throttling, which can incur large spillage drag. The comparison of spillage drag during throttling is shown in Figure 16. The definition of relative spillage drag (R_{spillage}) is shown in (6), where F_{spillage} is the spillage drag and $F_{\mathrm{uninstall}}$ is the uninstalled thrust.

$$R_{\mathrm{spillage}} = \frac{F_{\mathrm{spillage}}}{F_{\mathrm{uninstall}}}. \tag{6}$$

Since the airflow is kept constant during the constant-airflow throttling, the spillage is also kept constant. R_{spillage} increases as the uninstalled thrust drops during throttling. It increases from 1.17% to 1.94% during the subsonic throttling and increases from 0.18% to 0.29% during the supersonic throttling. However, the airflow decreases during the reduced-airflow throttling, incurring the increase of spillage drag and more increase of R_{spillage}. It increases from 1.17% to 6.87% during the subsonic throttling and increases from 0.18% to 7.22% during the supersonic throttling. Compared with the reduced-airflow throttling, the spillage drag is reduced through maintaining airflow during the constant-airflow throttling, which results in the improvement of installed thrust and SFC. The comparison of installed thrust and SFC during throttling is shown in Figures 17 and 18. To compare with the result of three-bypass ACE discussed in the literature [4], the definition of relative installed thrust (R_F) and relative installed SFC (R_{SFC}) is kept the same as the literature [4]. The definition is shown in (7) and (8), where F_{install} is the installed thrust, $F_{\mathrm{correction}}$ is the corrected

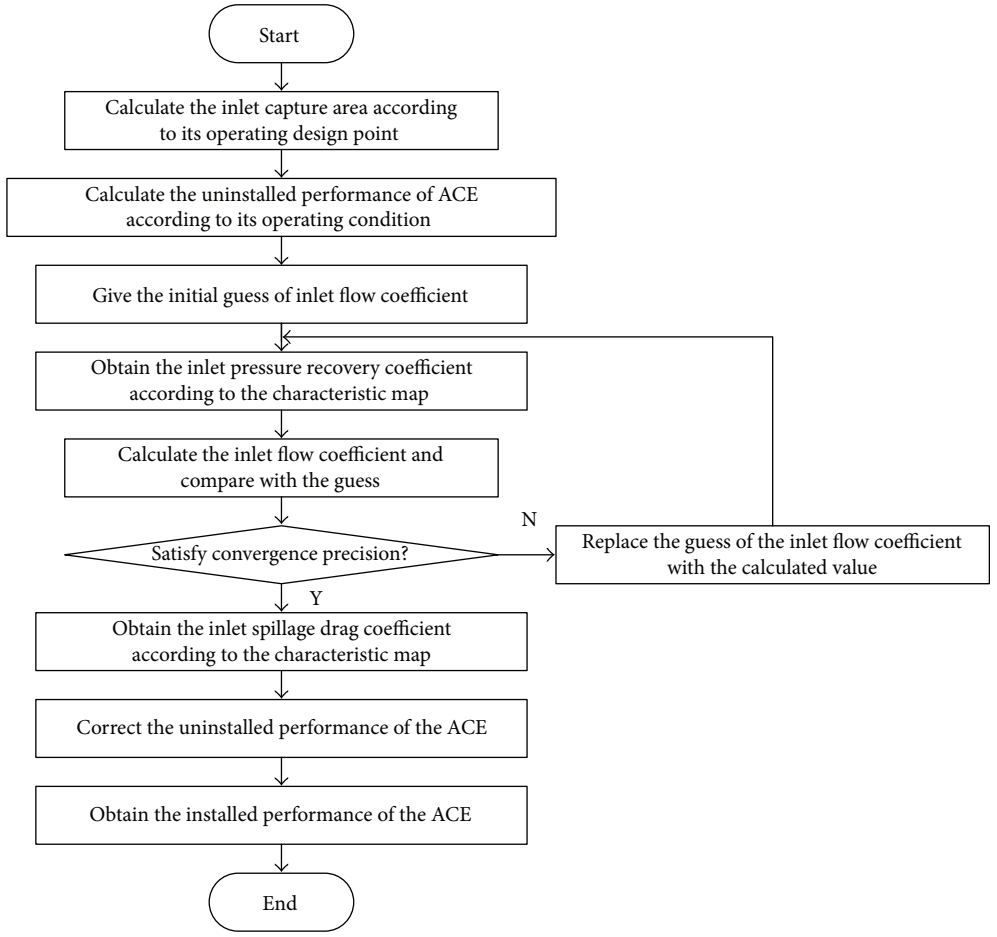

Figure 12: Installed performance calculation flowchart.

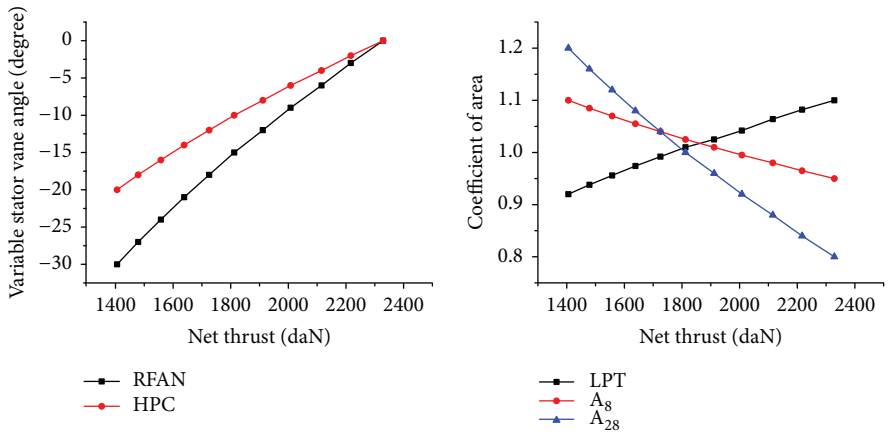

Figure 13: Control schedule of variable geometries (11 km, 0.8 Ma).

thrust, SFC_{actual} is the actual installed SFC, and $SFC_{initial}$ is the initial installed SFC.

$$R_F = \frac{F_{install}}{F_{uninstall}} = \frac{F_{correction} - F_{spillage}}{F_{uninstall}}, \quad (7)$$

$$R_{SFC} = \frac{SFC_{actual}}{SFC_{initial}}. \quad (8)$$

R_F decreases with the increase of $R_{spillage}$ during constant-airflow throttling. It decreases from 98.83% to 98.06% during the subsonic throttling and decreases from 99.82% to 99.71% during the supersonic throttling. However, R_F decreases more during reduced-airflow throttling due to the larger spillage drag. R_F decreases from 98.83% to 93.13% during the subsonic throttling and decreases from 99.82% to 92.78% during the supersonic throttling. Therefore, compared with R_F

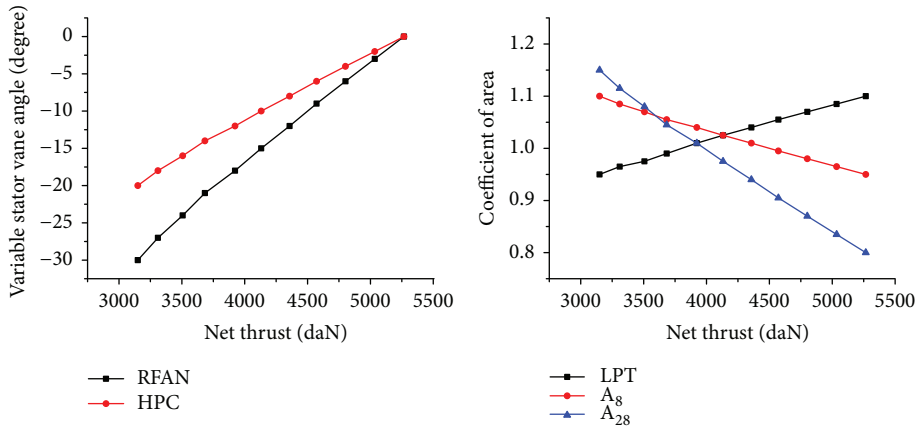

Figure 14: Control schedule of variable geometries (11 km, 1.5 Ma).

Table 9: Important performance parameters during throttling.

	R_F	π_{FFAN}	W_{aFFAN} (kg/s)	π_{RFAN}	W_{aRFAN} (kg/s)	π_{HPC}	W_{aHPC} (kg/s)	V_{28} (m/s)	V_9 (m/s)
0.8 Ma	100%	1.61	53.70	2.10	41.24	10.32	33.68	309.0	755.7
	60.36%	1.57	53.71	1.48	35.41	7.86	18.16	308.3	570.7
1.5 Ma	100%	1.61	113.21	2.08	86.71	10.23	70.95	350.1	1014.0
	59.81%	1.59	113.24	1.47	75.58	8.21	41.18	349.6	819.5

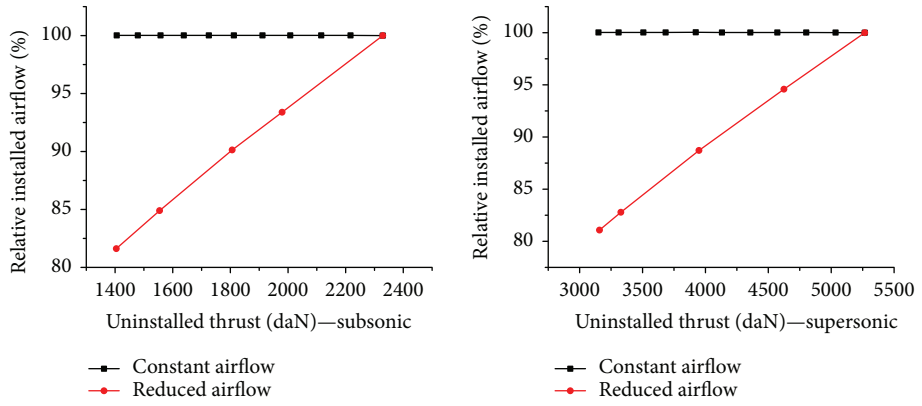

Figure 15: Variation of installed airflow during throttling.

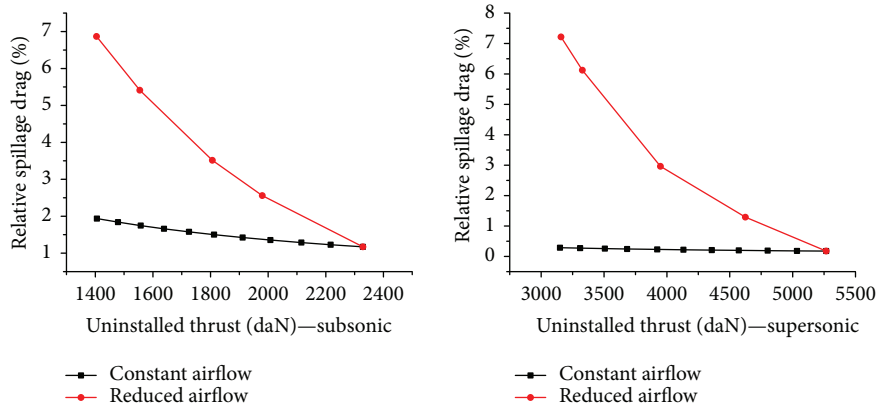

Figure 16: Variation of spillage drag during throttling.

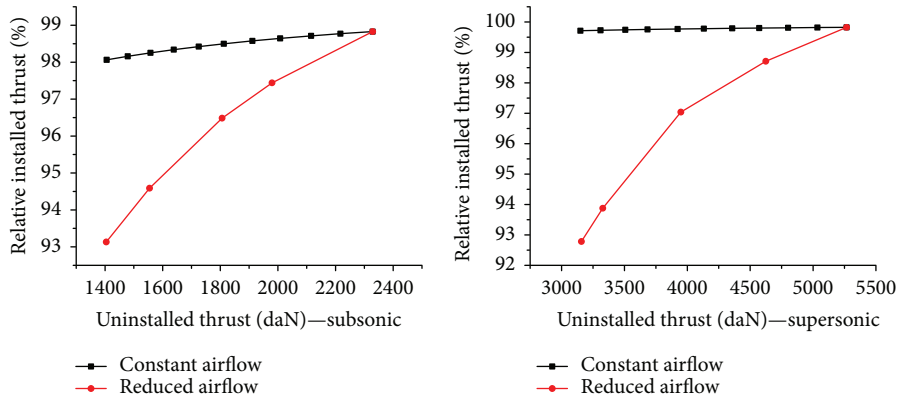

Figure 17: Variation of installed thrust during throttling.

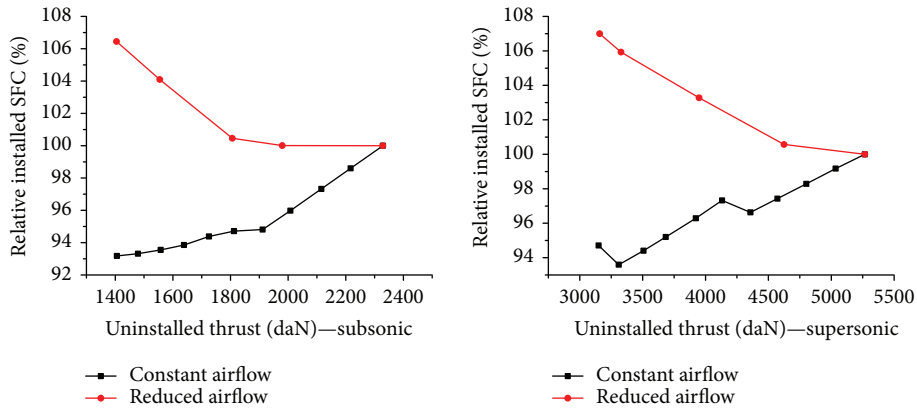

Figure 18: Variation of installed SFC during throttling.

during the reduced-airflow throttling, it increases by 4.93% during the subsonic constant-airflow throttling and by 6.93% during the supersonic constant-airflow throttling.

The definition of installed SFC is shown in (9), where $W_{f,\text{install}}$ is the installed fuel flow. It is determined by the installed fuel flow and installed thrust, which both decrease during throttling. The installed thrust drops slower than the installed fuel flow during constant-airflow throttling, which makes the installed SFC tend to drop. It decreases from 100% to 93.18% during the subsonic throttling and to 94.71% during the supersonic throttling. However, there are some kinks in the constant-airflow plots during the supersonic cruising, where the installed thrust drops faster than the installed fuel flow, resulting in the increase of installed SFC. This abnormal decrease of installed thrust is related to the gross thrust coefficient of the nozzle, which is related to the expansion ratio of the nozzle and the area ratio of the nozzle (the ratio of the nozzle exit area to the nozzle throat area). During the reduced-airflow throttling, the installed thrust drops faster than the installed fuel flow due to the spillage drag, resulting in the increase of installed SFC. It increases from 100% to 106.45% during the subsonic throttling and to 107.00% during the supersonic throttling. Therefore, compared with R_{SFC} during reduced-airflow throttling, it decreases by 13.27% during the subsonic constant-airflow throttling and by 12.30% during the supersonic constant-airflow throttling.

$$\text{SFC}_{\text{install}} = \frac{W_{f,\text{install}}}{F_{\text{install}}}. \tag{9}$$

4.2. Installed Performance Comparison of Two Types of ACE. The improvement of installed performance during throttling of the three-bypass ACE is discussed in the literature [4], including the improvement of installed thrust and installed SFC. The improvement of installed performance of the three-stream ACE and the three-bypass ACE is summarized in Table 10, where the values denote the comparison of installed performance during constant-airflow throttling and reduced-airflow throttling.

As the results show, the installed performance of the three-bypass ACE is improved more than the three-stream ACE's, especially during the subsonic throttling. It is a reasonable result considering the more complex configuration and control schedule of three-bypass ACE. Different from the three-stream ACE, it has the CDFS which is an important variable geometry during throttling. What is more, it has two operating modes which make it feasible to realize deeper throttling.

Table 10: Comparison of improvement of installed performance.

	Three-stream ACE		Three-bypass ACE	
	Installed thrust	Installed SFC	Installed thrust	Installed SFC
Subsonic	+4.93%	−13.27%	+11.06%	−27.17%
Supersonic	+6.93%	−12.30%	+8.53%	−18.25%

Table 11: Comparison of uninstalled thrust variation range.

	Three-stream ACE		Three-bypass ACE	
	Higher bound	Lower bound	Higher bound	Lower bound
Subsonic	100%	60.36%	100%	45.10%
Supersonic	100%	59.81%	100%	68.31%

The uninstalled thrust variation ranges of the three-stream ACE and three-bypass ACE is summarized in Table 11. During the subsonic throttling, three-bypass ACE operates at double bypass mode with a lower bypass ratio at first. Then, it transforms to triple bypass mode with a higher bypass ratio in order to make the uninstalled thrust reduce further. Benefiting from the double operating modes, three-bypass ACE can modulate the uninstalled thrust in a wider range during the subsonic throttling. However, the three-bypass ACE can only operate at double bypass mode during the supersonic throttling. What is more, the bypass nozzle exit area of the three-bypass ACE is fixed, limiting its potential in constant-airflow throttling. Therefore, compared with the three-stream ACE, the three-bypass ACE has a narrower variation range of uninstalled thrust during the supersonic throttling.

Compared with the three-stream ACE, the three-bypass ACE has a wider variation range of uninstalled thrust during the subsonic throttling, resulting in more improvement of installed performance. What is more, the CDFS also has great effect on the improvement of three-bypass ACE's installed performance. The adjustment of the variable stator vane of the CDFS (VSV_{CDFS}) changes the flow capacity of the CDFS directly, which affects the distribution of HPR's compression work and the back pressure of the RFAN. Through the proper adjustment of VSV_{CDFS} during throttling, the HPRS of the three-bypass ACE is kept at a higher value and drops more slowly compared with the HPRS of the three-stream ACE, which is shown in Figure 19. When the uninstalled thrust of three-bypass ACE decreases to about 65% during the subsonic throttling, its operating mode transforms from double bypass mode to triple bypass mode, resulting in some kinks on the black curve in the left plot. The higher and stable HPRS of the three-bypass ACE makes the CDFS and HPC operate with high efficiency. What is more, benefitting from the improvement of HPRS, three-bypass ACE's RSR is also kept at a higher value compared with the RSR of the three-stream ACE. The higher RSR improves the surge margin of FFAN and RFAN. Finally, the improvement of components' efficiency and surge margin results in better installed performance for three-bypass ACE.

Therefore, benefitting from the double operating modes and the adjustment of VSV_{CDFS}, the three-bypass ACE can achieve better potential in maintaining the airflow during throttling. The uninstalled thrust variation range of the three-bypass ACE is wider during the subsonic throttling, and the components' surge margin and efficiency is improved, resulting in its advantage of installed performance over the three-stream ACE during throttling. However, this advantage is achieved at the cost of more complex configuration and control schedule.

Compared with the three-bypass ACE, the three-stream ACE is not equipped with the CDFS, which is a significant component of the three-bypass ACE and is one of the greatest challenges during the design stage, because it has to operate efficiently within a wide range of power [23, 24]. What is more, the configuration of the three-stream ACE is more similar with the traditional type of engine, such as turbofan. It can be regarded as a mixed turbofan equipped with a front fan stage and an outer bypass duct. Therefore, it is easier to be derived from the existing versatile turbofans than the three-bypass ACE.

As for the design of control schedule, the technical difficulty of the three-stream ACE is less than three-bypass ACE's. Firstly, the throttling process of the three-stream ACE is controlled by five variable geometries, while the three-bypass ACE is controlled by six variable geometries. What is more, three-stream ACE has only one operating mode and does not need to take the mode transition into consideration during throttling. However, the mode transition is necessary during the subsonic throttling of the three-bypass ACE to achieve a wider variation range of uninstalled thrust. In order to complete the mode transition smoothly and safely, the control schedule should be designed to guarantee constant airflow, constant thrust, and enough surge margins during this process, which is another great challenge during the design stage [36].

In summary, the three-stream ACE is a compromise design considering the technical risk and the variable cycle characteristic. The improvement of its installed performance is less than the three-bypass ACE's during throttling, but it is less complicated and is easier to be designed. Considering the technical feasibility, three-stream ACE is a better platform to verify the component technology and control schedule for further research, which can reduce the research cost and risk. With the technical progress in component and control system, the three-bypass ACE and other complex types of ACE are the better choices to achieve more improvement of installed performance and other variable cycle characteristics.

5. Conclusion

Maintaining the airflow through a combined control of variable geometries during throttling is an important variable cycle characteristic of the ACE, which improves the spillage drag of the engine, resulting in the improvement of installed performance. This article analyzes the performance of a three-stream ACE during the subsonic cruise throttling and

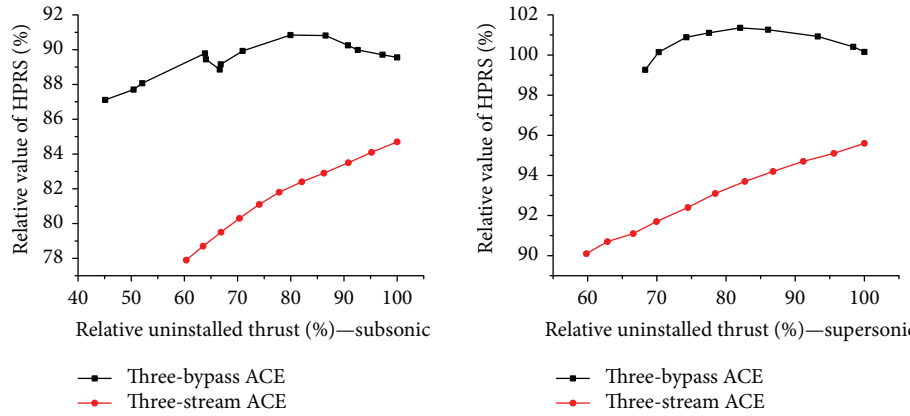

Figure 19: Variation of HPRS during throttling.

supersonic cruise throttling, including the selection scheme analysis of variable geometries and the comparison analysis with a three-bypass ACE. The important conclusions are summarized as follows.

(1) It is unnecessary to take the risk of installing the variable geometries into VABI and the stator vane of HPT, considering that their effect on modulating throttling can be replaced by the other five variable geometries. Through the combined control of VSV_{RFAN}, VSV_{HPC}, VAN_{LPT}, A_8, and A_{28}, the uninstalled thrust can reduce from 100% to 60.36% during the subsonic cruise and to 59.81% during the supersonic cruise.

(2) Through maintaining airflow during throttling, the spillage drag is decreased to some degree compared with the reduced-airflow throttling, resulting in the improvement of installed thrust and installed SFC.

(3) The improvement of installed performance of the three-stream ACE is less than the three-bypass ACE's. However, the configuration of the three-stream ACE is more similar with the traditional type of engine, which makes it easier to be derived from the existing versatile turbofans. What is more, the three-stream ACE has only one operating mode and less variable geometries, which makes its control schedule simpler.

Three-stream ACE is a compromise design considering the technical risk and variable cycle characteristic. It is a good platform to verify the component technology and control schedule of the ACE. Based on the technical progress in component and control system, the ACE with more complex configuration can be researched at a lower technical risk.

Conflicts of Interest

The authors declare that they have no conflicts of interest.

Acknowledgments

This research is funded by the National Nature Science Foundation of China (NSFC) under Grants 51206005 and 51776010. The authors are thankful for the support from the Collaborative 341 Innovation Center of Advanced Aero-Engine.

References

[1] L. Bin, C. Min, Z. L. Zhu, and Z. Kun, "Steady performance investigation on various modes of an adaptive cycle aero-engine," *Journal of Propulsion Technology*, vol. 34, no. 8, pp. 1009–1015, 2013.

[2] J. Zheng, M. Chen, and H. Tang, "Matching mechanism analysis on an adaptive cycle engine," *Chinese Journal of Aeronautics*, vol. 30, no. 2, pp. 706–718, 2017.

[3] Y. Lyu, H. Tang, and M. Chen, "A study on combined variable geometries regulation of adaptive cycle engine during throttling," *Applied Sciences*, vol. 6, no. 12, 2016.

[4] Y. Lyu, *Study on Performance of Adaptive Cycle Engine, [M.S. thesis]*, Aerospace Propulsion Theory and Engineering, Beihang University, Beijing, China, 2016.

[5] J. Zheng, H. Tang, M. Chen, and F. J. Yin, "Equilibrium running principle analysis on an adaptive cycle engine," *Applied Thermal Engineering*, vol. 132, pp. 393–409, 2018.

[6] D. R. Ballal and J. Zelina, "Progress in aeroengine technology (1939–2003)," *Journal of Aircraft*, vol. 41, no. 1, pp. 43–50, 2004.

[7] S. N. B. Murthy and E. T. Curran, "Variable cycle engine developments at general electric-1955–1995," in *Developments in High-Speed Vehicle Propulsion Systems*pp. 105–158, American Institute of Aeronautics and Astronautics, Reston, VA, USA.

[8] J. Johnson, "Variable cycle engines - the next step in propulsion evolution," in *12th Propulsion Conference*, pp. 1–38, Palo Alto, CA, USA, July 1976.

[9] J. Kurzke, "The mission defines the cycle: turbojet, turbofan and variable cycle engines for high speed propulsion," NATO, Brussels, Belgium, 2010.

[10] P. Dong, H. Tang, and M. Chen, "Study on multi-cycle coupling mechanism of hypersonic precooled combined cycle

engine," *Applied Thermal Engineering*, vol. 131, pp. 497–506, 2018.

[11] P. Dong, H. Tang, M. Chen, and Z. Zou, "Overall performance design of paralleled heat release and compression system for hypersonic aeroengine," *Applied Energy*, vol. 220, pp. 36–46, 2018.

[12] J. W. Vdoviak, P. R. Knott, and J. J. Ebacker, "Aerodynamic/acoustic performance of YJ101/double bypass VCE with coannular plug nozzle," NASA, Cincinnati, OH, United States, 1981.

[13] M. A. R. Do Nascimento and P. Pilidis, "The selective bleed variable cycle engine," in *ASME 1991 International Gas Turbine and Aeroengine Congress and Exposition*, pp. 1–7, Orlando, FL, USA, June 1991.

[14] J. S. Westmoreland, R. A. Howlett, and R. P. Lohmann, "Progress on variable cycle engines," in *AIAA/SAE/ASME 15th Joint Propulsion Conference*, pp. 1–10, Las Vegas, NV, USA, 1979.

[15] P. Vyvey, W. Bosschaerts, V. F. Villace, and G. Paniagua, "Study of an airbreathing variable cycle engine," in *47th AIAA/ASME/SAE/ASEE Joint Propulsion Conference & Exhibit*, pp. 1–10, San Diego, CA, USA, July 2011.

[16] H. Zhou, Z. Wang, X. Zhang, and M. Cao, "Optimization of variable cycle engines by using an improved differential evolution," in *50th AIAA/ASME/SAE/ASEE Joint Propulsion Conference*, pp. 1–10, Cleveland, OH, USA, July 2015.

[17] M. A. R. Nascimento and P. Pilidis, "An optimisation-matching procedure for variable cycle jet engines," in *ASME 1992 International Gas Turbine and Aeroengine Congress and Exposition*, pp. 1–10, Cologne, Germany, June 1992.

[18] R. J. Simmons, *Design and Control of a Variable Geometry Turbofan with an Independently Modulated Third Stream, [Ph.D. thesis]*, Aerospace Engineering, Ohio State University, Columbus, OH, USA, 2009.

[19] H. R. Patel, *Parametric Cycle Analysis of Adaptive Cycle Engine, [M.S. thesis]*, Aerospace Engineering, The University of Texas at Arlington, Arlington, TX, USA, 2016.

[20] J. J. Berton, W. J. Haller, P. F. Senick, S. M. Jones, and J. A. Seidel, "A comparative propulsion system analysis for the high-speed civil transport," NASA, Cleveland, Ohio, United States, 2005.

[21] Y. Xu, M. Chen, and H. L. Tang, "Preliminary design analysis of core driven fan stage in adaptive cycle engine," in *53rd AIAA/SAE/ASEE Joint Propulsion Conference*, pp. 1–12, Atlanta, GA, USA, July 2017.

[22] X. Meng, Z. L. Zhu, and M. Chen, "Steady-state performance comparison of two different adaptive cycle engine configurations," in *53rd AIAA/SAE/ASEE Joint Propulsion Conference*, pp. 1–11, Atlanta, GA USA, July 2017.

[23] M. Dodds and P. Pilidis, "The influence of a variable capacity turbine in the performance of a variable cycle engine," in *ASME 1999 International Gas Turbine and Aeroengine Congress and Exhibition*, pp. 1–8, Indianapolis, IN, USA, June 1999.

[24] X. Zhang and B. J. Liu, "Analysis of aerodynamic design characteristics of core driven fan stage," *Journal of Aerospace Power*, vol. 25, no. 2, pp. 434–442, 2010.

[25] X. Zhang and B. J. Liu, "Investigation of a methodology for core driven fan stage matching in the off-design mode," *Journal of Propulsion Technology*, vol. 35, no. 3, pp. 320–327, 2014.

[26] Z. Yueliu and W. Yuan, "Analysis of aerodynamic design characteristics of flade fan," *Procedia Engineering*, vol. 99, pp. 723–733, 2015.

[27] P. P. Walsh and P. Fletcher, "Off design performance," in *Gas Turbine Performance*, vol. 391p. 393, Blackwell Science Ltd, Oxford, UK, 2nd edition, 2004.

[28] M. Chen, Z. L. Zhu, D. M. Zhu, J. Zhang, and H. L. Tang, "Performance analysis tool for turbine based combined cycle engine concept," *Journal of Astronautics*, vol. 27, no. 5, pp. 854–859, 2006.

[29] H. L. Tang and J. Zhang, "A study of object-oriented approach for aeroengine performance simulation," *Journal of Aerospace Power*, vol. 14, no. 4, pp. 421–424, 1999.

[30] H. L. Tang, M. Chen, D. H. Jin, and Z. P. Zou, "High altitude low Reynolds number effect on the matching performance of a turbofan engine," *Proceedings of the Institution of Mechanical Engineers, Part G: Journal of Aerospace Engineering*, vol. 227, no. 3, pp. 455–466, 2013.

[31] C. Min, H. L. Tang, K. Zhang, O. Y. Hui, and Y. J. Wang, "Turbine-based combined cycle propulsion system integration concept design," *Proceedings of the Institution of Mechanical Engineers, Part G: Journal of Aerospace Engineering*, vol. 227, no. 7, pp. 1068–1089, 2012.

[32] W. H. Ball and T. E. Hickcox, "Rapid evaluation of propulsion system effects, Vol. IV, library of configurations and performance maps," AD B031555, Seattle, WA, United States, 1978.

[33] E. J. Kowalski, "Computer code for estimating installed performance of aircraft gas turbine engines. Volume 1: final report," NASA CR-159691, Seattle, WA, United States, 1979.

[34] E. J. Kowalski, "Computer code for estimating installed performance of aircraft gas turbine engines. Volume 2: users manual," NASA CR-159692, Seattle, WA, United States, 1979.

[35] E. J. Kowalski, "Computer code for estimating installed performance of aircraft gas turbine engines. Volume 3: library of inlet/nozzle configurations and performance maps," NASA CR-159693, Seattle, WA, United States, 1979.

[36] U. T. J. Grönstedt and P. Pilidis, "Control optimization of the transient performance of the selective bleed variable cycle engine during mode transition," *Journal of Engineering for Gas Turbines and Power*, vol. 124, pp. 75–81, 2002.